
Article:
Caulkin, R, Tian, W, Pasha, M et al. (2015) Impact of shape representation schemes used in discrete element modelling of particle packing. Computers and Chemical Engineering, 76. 160 - 169. ISSN: 0098-1354

https://doi.org/10.1016/j.compchemeng.2015.02.015

Impact of shape representation schemes used in discrete element modelling of particle packing

Richard Caulkin, Wei Tian, Massih Pasha, Ali Hassanpour, Xiaodong Jia

Institute of Particle Science and Engineering, School of Process, Environmental and Materials Engineering, University of Leeds, Leeds LS2 9JT, UK

Corresponding author: Dr Richard Caulkin
Email: r.caulkin@gmail.com

Abstract

Details of particle shape, including surface roughness or texture, curvature or sharpness of surface features and edges, are known to have an impact on particle packing structure. In different computer models, shape is represented using different approaches to varying degrees of precision. Thus, it is to be expected that different approaches, or rather their precision of shape representation, can affect not only how computationally demanding the simulation model is but also how accurate the model prediction can be. This paper examines two different approaches to shape representation, and their effects on the accuracy of model predictions, in the context of non-spherical particle packing. To this end, two commercially available discrete element method (DEM) based software packages, EDEM and DigiDEM, are used. The former, referred to here as sphere-composite approach, represents one extreme where a shape is typically coarsely represented by clumping together a small number of primary spheres. The latter, known as voxel-based approach, represents the other extreme where a shape is typically finely represented by a huge number of voxels (3D pixels). Both are used to simulate packing of cylinders – the most common shape of catalyst pellets in packed column reactors widely used in chemical, oil refinery and process industries. Previously reported X-ray CT scan of a packed bed provides the experimental measurements for both to compare with, in terms of bulk packing fraction, axial and radial packing fraction profiles, and pellet orientation distributions. Eight sphere-composite representations of the same cylindrical pellet were tested. Two of them gave results that quantitatively (i.e., within 5% margin of error) follow experimental measurements. A range of factors that in theory could affect accuracy of the simulation results have been examined in detail, including edge roundedness, surface roughness and restitutional behaviour as a function of sphere-composite representations. The conclusion therefore is that, for packing at least, matching the object's overall shape and dimensions is not enough, only when a high enough resolution is applied to corners and edges, could the sphere-composite approach possibly

match the experimental data quantitatively.

1. Introduction

Particle shape can have a significant influence over packing structure and it plays an important role in the behaviour of a multitude of particulate systems (Santamarina 2004). Packing is a wide reaching phenomenon that occurs in both nature and in industry. Packing of spheres is well studied (Aste & Weaire, 2008), but increasingly non-spherical (i.e., more realistically shaped) particles are being packed in numerical simulations. A notable example is randomly packed columns used as chemical reactors. Simulations of packing structure, flow and mass transfer in packed columns used to be almost exclusively sphere based (Powell, 1980; McGreavy et al. 1986; Kubie, 1988), but the focus is being now shifted to real (non-spherical) shapes. This has been enabled by two specific technical advances, in addition to increasing computing power. One is the commercial availability of software tools that are specifically designed to handle and model the behaviour of non-spherical complex shapes. The other is the availability of affordable tomographic imaging devices, such as X-ray micro-tomography (XMT) and magnetic resonance imaging (MRI) systems. Packed columns can be explored using X-ray Tomography (Seidler et al. 2000, Philippe et al. 2003) or Magnetic Resonance Imaging (Sharma et al. 2001) to investigate the positions and orientations of particles within it. However, it is more convenient to employ validated numerical methods to simulate the particle movement due to costs, effort and freedom of selecting particle characteristics such as shape and particle size distribution (PSD).

The Distinct Element Method (DEM) first proposed by Cundall and Strack (1979) has become a standard numerical simulation methodology for modellers dealing with all kinds of particulates. In all software implementations of DEM, the basic procedure is the same: the forces acting on each individual particle are evaluated, Newton's equations of motion are solved, typically using the finite difference method (FDM), in a (time) step by step fashion, to update each particle's velocity and position, from which behaviour of the assembly is derived. A main difference between different DEM implementations is how particles, or rather their shapes, are represented. This difference necessarily leads to algorithmatically different ways of collision/overlap detection and to some extent contact force calculation. To represent a non-spherical shape, three main generic approaches currently exist: sphere-composite, surface-mesh and voxel-based. A brief commentary of their differences is given in Table 1. It may be worth pointing out that analytical representation is excluded from the above for not being a truly 'generic' approach since it is restricted to simple shapes (e.g., ellipsoids) and the ones (e.g., spherical harmonics) that can be mathematically morphed from a base shape.

TABLE 1

Further to Table 1, the principal differences between sphere-composite models and voxel-based approaches that should be emphasised are:

(1) Voxel-based models use a large number of voxels (typically 10K-100K per object, and 50M or more voxels per simulation); and digitised shapes often come directly from CT scans of real objects. For sphere-composite models,

because of the obvious speed penalty, the tendency is to use as few spheres as possible, hence the common practice of hand-crafting each shape. Level of details of the two approaches is clearly very different.

(2) Primary spheres are allowed to partially overlap with each other, such that a sphere-composite object can easily be made to match precisely with the dimensions of the real object. Voxel-based digital representation on the other hand often cannot have an exact match. Even though the difference is within one voxel width along each axis, it can be significant if the digital object is small (e.g., one voxel difference for a 10-voxel wide object means up to 10% margin of error).

(3) Since voxel-based approach is already using a huge number of voxels, a more complex shape does not necessarily mean more voxels required, and a simpler shape does not necessarily mean fewer voxels required. For example, a solid sphere needs much more voxels to construct than a fractal-like agglomerate of the same linear dimension. By contrast, sphere-composite approach usually does require more primary spheres to build up a more complex shape. In this sense, the more complex the shapes are, the more advantageous the voxel-based approach is expected to become.

(4) Computationally, voxels do not rotate with the object they represent, they merely relocate in the lattice grid. An analogy is the pixels on a computer screen versus the image a tumbling object shown on the screen. Because of this, even though the voxel-based approach uses a much larger number of building blocks (voxels), simulation runtime is not necessarily longer than the sphere-composite approach.

(5) A typical sphere-based DEM model has a wider choice of contact force models than the voxel-based DEM. This is because regardless of the shapes sphere-composites represent, contact force is calculated between pairs of spheres and sphere-sphere contact mechanics is the most extensively studied. By contrast, voxel-based DigiDEM calculates contact force at object-level, and contact force models between arbitrary shapes are much limited. voxel-based DigiDEM deals with contact between arbitrary shapes. In DigiDEM, contact force is assumed to be proportional to overlap volume.

The above differences beg a question which to our knowledge remains largely unanswered: how do different shape representation approaches compare in a real application? In the present paper an attempt is made to compare two of them (sphere-composites and voxel-based approaches),for the packing of uniform cylindrical particles in a packed column setup. We do not have access to DEM code based on a surface mesh approach; both DEM programs (sphere-composite based EDEM and voxel-based DigiDEM) used in this study are commercially available. The motivation for choosing cylinders is threefold:

- it is a generic shape for pellets in most packed column reactors hence its practical significance;
- it captures geometric features (flat surface, curved surface and sharp corners) common to most shapes hence applicability of the conclusions drawn from the study can be expected to be wider than the specific shape (cylinder) used; and
- it is simple enough to for shape related characteristics to be calculated analytically hence the relative ease for accuracy analysis at single-particle geometry level.

The accuracy of simulation results at bed level (i.e., packing structure) is assessed against previously published experimental data (Caulkin et al. 2009b) obtained from XMT scans of an identical packed column.

2. Materials and methods

The clumped spheres method is a technique for shape representation which is suggested by many researchers (Favier et al. 1999) and is utilised by a number of software packages such as PFC2D and PFC3D, LIGGGHTS and EDEM. In this study we utilise the EDEM package (from DEM Solutions) for the clumped sphere method, while the voxel-based DEM software used was DigiDEM (from Structure Vision). Algorithmatic details of both software tools used in this work have been amply documented elsewhere (EDEM: Guises et al. 2009; DigiDEM: Xu et al. 2006, Caulkin et al. 2009b), and will not be laboured here. Setups for XMT experiment and voxel-based (DigiDEM) simulation are briefly repeated here, followed by details of sphere-cluster (EDEM) setups. Other relevant features of the simulation models will be mentioned along with discussion of the results.

2.1 XMT

For experimental data reported in this work, a Phoenix Nanatom CT scanner was used to determine packing structure. Details have been reported elsewhere (Caulkin et al. 2009b), only the most pertinent points are repeated here. The pellet shape used in the present study for comparison is that of A38 pellets: cylindrical alumina pellets 3.46 mm in height and 3.42 mm in diameter with flat ends, packed in a cylindrical tube of 44.5 mm internal diameter. The Nanotom is a 160-kV nanofocus CT scanner, equipped with a 5-megapixel (2304 × 2304 pixels) CCD detector. The scan resolution was 0.024 mm, but reconstruction was done at 1/4 scale. Thus, reconstructed images had a pixel resolution of 0.096 mm. Because of experimental limitations (namely, the height of the real packed columns), the full height of the bed could not be fully accommodated by the view area. Therefore XMT-scanned structures were applied to axial density profiles only in the central region of the packing, ignoring the regions near the base wall and the top of the column. The reason for this is because bulk structure is of the most practical interest for packed columns (which, in real applications, can be 10 m high but only several inches wide), from which mean bulk density measurements were to be calculated, it was considered vital to achieve a span that was expansive enough to provide a representative sample for reliable analysis. A total of five repeat packings and subsequent scans were undertaken to gain representative results for the given cylindrical pellets.

2.2 Voxel-based method

Details of DigiDEM algorithm and simulation setups have too been reported elsewhere (Xu et al. 2006, Caulkin et al. 2009b) and only the most significant aspects are recited here. For the sake of simulation runtime, while keeping digitisation errors to a reasonable level (aspects of which have been previously reported (Caulkin et al. 2014)) the pellet shape was represented digitally by a voxelated cylinder 17 pixels wide and 18 pixels high (resolution = 0.197 mm/pixel). In other words, each pellet contained 4050 voxels. By volume, the digital version

was 0.8% smaller than the mathematically perfect cylinder it was meant to represent. Typical runtime on a PC with an Intel Xeon 2.66 GHz CPU was 22 hours to achieve final distribution.

2.3 Clumped-sphere method

Packing structures of cylindrical particles in a container with diameter of 44.5 mm and height of 120 mm are simulated to recreate the set-up conditions of the experimental beds. Cylindrical particles with diameter of 3.42 mm and a height of 3.46 mm are built by combining clusters of spheres. Typical runtime of EDEM simulations was 20 hours for 0.8 s of real time. Eight different representations of the same generalised particle shape are considered, shown in Figure 1. These representations differ in the total number of element spheres as well as in terms of the size of the element spheres. The configurations of the size and number of element spheres are summarised in Table 2. Typical time to properly construct these shapes was 3 hours, and typical EDEM runtime was 20 hours (for 0.8 s of real packing time).

It is important to note that even though different sizes of spheres and different levels of overlap are used to construct the representations, all of them produce particles with uniform dimensions (height and length). Different representations however do have differing degrees of "roundness" for the edges and "roughness" for the top and side surfaces. The effects of these criteria upon packing data are investigated more closely in the next section.

FIGURE 1
TABLE 2

Following simulated pellet packing, whereby particles were randomly placed in the column and then allowed to settle, axial density fraction was calculated as thus; the cylindrical container was divided into 18 equal sections over the height of container and the volume of particles and the number of particles in each section were determined. The total volume of representation was calculated by multiplying the number of particles by the corrected volume of particles. The corrected volume of a single particle is equal to the real alumina cylinder used in laboratory experiments. The packing volume fraction in each section is then the ratio of the particle volume of particles in that section to the overall volume of the section. For radial density fraction, the bed was divided into seven equally spaced concentric rings. Each section had a different volume, depending on the distance from the centre. The values of volume for each section are $4.95\text{x}10^{-5}$ m^3, $4.19\text{x}10^{-5}$ m^3, $3.42\text{x}10^{-5}$ m^3, $2.67\text{x}10^{-5}$ m^3, $1.90\text{x}10^{-5}$ m^3, $1.14\text{x}10^{-5}$ m^3 and $3.81\text{x}10^{-6}$ m^3. The corrected volume of particles and the volume packing fraction is evaluated in the same manner as for the axial density fraction. If a particle overlapped the boundary section, then the position of the particle was determined by the location of the particle centre. More accurate calculation was made to define the error caused by this effect. Orientation of each particle at different time steps is exportable. The orientation of each particle is determined from nine values which are expressed in tensor. The nine values (xx, xy, xz, yx, yy, yz, zx, zy, zz) represent a 3*3 matrix which is the rotation from the particle co-ordinate system to the global co-ordinate system. Assuming that z-local is the vertical axis of a cylinder, the last value zz is used to calculate the angle between a pellet and the vertical axis (Angle = 180*acos(zz)/PI).

3. Results and Discussion

3.1 Clumped sphere method – comparison of the effects of resolution

Figures 2 and 3 show the trends of radial and axial packing fraction respectively of the packed beds investigated using the clumped sphere method for the eight cylinder representations.

FIGURE 2
FIGURE 3

As indicated in Figures 2 and 3, the trend of radial and axial volume packing fraction is the same for all the eight different representations. For radial packing density, solid packing fraction at the container wall is reduced compared to the rest of the bed, as denoted by the rapid increase in packing fraction between 0 and 1 particle diameters. This is attributable to wall effects. Damped cyclic variation of packing fraction in the radial direction is a common occurrence in beds packed with mono-sized particles as one moves from the bed wall to its centre. This phenomenon typically extends a couple of particle diameters into the bed before it becomes negligible. It is therefore an important factor in beds with low tube-to-particle diameter ratios. Beyond two particle diameters from the wall (Figure 2), the volume fraction for respective cylinder representations is found to be largely stable, suggesting packing is relatively uniform within the bulk of the bed. In terms of axial volume packing fraction, the packing density is also stable within the bulk of the bed. End effects, which can be defined as the trend whereby the mean packing fraction increases with increasing bed length extend for a maximum of two particle diameters into the packing from the base of the container. Beyond this, they are observed to have all but dissipated, with only small, natural fluctuations caused by particle-particle boundary contacts. The values of both radial and axial volume packing fractions differ significantly between the different pellet representations, with those pellets constructed using smaller sphere radii producing lower overall packing fractions. The results were expected to be the same or very similar in all numerical experiments, because the eight cylindrical representations were designed to have essentially the same external physical dimensions. The results indicate that the radii of the element spheres which are used to build individual particles and ways the element spheres are clustered affect the packing within the column to a notable degree. To investigate this in more detail, "roundness" (i.e., curvature and sharpness of the edges) and "roughness" of the shape representations, not of the real particles they represent, and particle dynamics are evaluated for each of the 8 cases.

3.2 Roundness

From the 8 cases reported (Figure 1), the trend in radial and axial packing fractions (Figures 2 & 3) indicate that when larger primary spheres are used to cluster-build a cylinder pellet, higher packing densities are the outcome. A possible explanation for this is that it is roundness that influences packing structure. Kodam et al. (2009) and Höhner et al. (2011) defined particle roundness as D_s/D_i (Figure 4) which is the ratio of the diameter of sphere that fits the

sharpest corner to that of the diameter of largest sphere which can be inscribed in the particle. It is intended as a measure of curvature and how sharp the edges of the ends of the cylinders are for each of the 8 sphere-composite representations, and how this relates to bulk packing fraction. The maximum diameter of sphere which could be inscribed in each particle composite is 3.42 mm. The values of roundness and volume packing fraction are listed in Table 3.

FIGURE 4
TABLE 3
FIGURE 5

It can be drawn from the values reported in Figure 6 that the volume packing fraction generally follows roundness. As roundness increases, the bulk packing fraction values asymptote out to a higher than expected value. This is to be expected, since rounded corners allow objects to come closer than otherwise. Analogous phenomenon have also been reported in several other works (Shimobe 1995; Dyskin, Estrin et al. 2001; Jia and Williams 2001) where sharp corners can prevent particle rotation and mobility, thus decreasing packing volume fraction. A subsequent group of simulations are reported to confirm the result pattern. The shapes of selected representations were marginally altered by adding a layer of 0.342 mm radius spheres at both ends of the original representations while maintaining the same overall diameter and height as the eight representations originally reported (Figure 1). The respective modified cylinder composites have uniform roundness, however, the roughness is different between each representation. A marked decrease in radial packing fraction occurred (Figure 6) for the modified particles from those of the respective original cylinder representations. For instance, mean radial packing fraction of the original representation with spheres of radius 0.74 mm was 0.685. For the modified particle based on this representation with edge of 0.34 mm spheres, the mean radial volume packing fraction is 0.596. Another occurrence is that the two modified representations (built using spheres with radii 0.47 mm and 0.74 mm) together with the original representation (0.34 mm, n=120 from Table 2, built using spheres with 0.34 mm radius) have comparable radial packing fractions. These three representations have the same roundness (D_s/D_i = 0.2) but differing roughness. From these numerical experiments the roundness of representations appears to be a determining factor that affects the packing structure.

FIGURE 6

3.3 Roughness

The method by which the component spheres are clustered when building a composite cylinder influences particle roughness. This section aims to identify the extent to which roughness affects the packing structure of the bed. In the cases reported (Figure 1) particles with radii of 0.84 mm, 0.8 mm and 0.74 mm were built using the same process of clustering (same number and layout of spheres). The primary difference (with the exception of different sphere sizes) is the degree of overlap between neighbouring spheres. Overlap was adjusted to ensure equal height and diameter (3.46mm and 3.42mm respectively) between each of the 8

examples of composite cylinders. From Figures 2 and 3, the radial packing densities and axial packing densities were comparable in these three cases (0.84mm, 0.8mm and 0.74mm).

FIGURE 7
TABLE 4

Quantification of roughness representation is indicated in Figure 7. Roughness is calculated as the distance between the two concentric circles (one of which circumscribes the representation and the second aligns the contacts of the outer layer of spheres). For the three examples mentioned (0.84mm, 0.8mm and 0.74mm) roundness (Table 3) and roughness (Table 4) do not change greatly and so neither do the radial and axial packing fraction results. However, in the comparing process, the factor of angularity was not excluded.

FIGURE 8

For particles with the same size of component spheres (representations 4 & 5 (0.47 mm) and representations 7 & 8 (0.34 mm)) which were clustered using different methods, the respective mean radial packing fractions differ only slightly despite the relatively large differences in roughness. The two composite particles built with spheres of radius 0.34 mm had the lowest overall packing densities of the 8 representations. According to the radial packing density and axial packing fractions (Figures 2 & 3), the packing structures for this example are analogous. The method used to cluster particles and the number of spheres used as 'building blocks' determines the roughness of particles, which has a secondary and relatively minor influence on packing structure when compared to roundness. In both the sphere-composite method and the voxel-based model friction is dealt with in a standard DEM way. No clear trend between roughness and mean bulk packing fraction was found in Figure 8, although the increased friction that results from higher roughness will make it more challenging for particles to move against one another and to rotate. Additionally, bulk packing fractions will generally be decreased as particles with higher degrees of roughness will create small, un-fillable voids between objects that are otherwise in close physical contact. Future studies should investigate particle representations with larger discrepancies in roughness to study the effect on the movement of particles in the clumped sphere method. Additionally, the effects of other criteria upon packing structure, such as different particle masses should be considered.

3.4 Dynamics

In numerical experiments packing structure is the result of individual particle movement, how they interact and how they eventually come to rest in contact with each other and the container. Each of the 8 sphere-composite particle representations was tested under the same conditions to investigate how such structures behave when they make contact with the flat bottom of the container. In the tests reported (Table 5), an individual particle was introduced in the centre of the cylindrical container at a fixed height above the base. The same position was used for each of the subsequent tests using different pellet representations. Two groups of tests were undertaken for each sphere-composite representation, one with an initial particle orientation angle of 2^o (i.e. near upright) and the other at an initial angle of 45^o.

TABLE 5

In all of the tests reported, particles made contact with the bottom of the container between 0.11s to 0.12s after introduction. For the particles with an initial angle of approximately 2^o (pellet in an upright position) the rebounding heights ranged from 0.00166 to 0.00465 (mean = 0.00271, stdev = 0.00096). The maximum rebound height (from the representation built using 0.74 mm radii spheres) is approximately three times that of the minimum rebound height (0.84 mm radii spheres). In the second group of tests, where the initial orientation angle was approximately 45^o the rebound height ranged from 0.00068 to 0.00719 (representations 0.8 mm and 0.57 mm respectively) Mean value of 45^o data = 0.00315; stdev = 0.00187. The orientations of the particles after making contact with the container base vary widely between the different cylinder representations, even for particles within the same 'initial angle' group. This effect was significantly more pronounced for the 45^o tests, which when analysed in the clumped sphere method, was observed that the representations behave significantly differently (between different representations and compared to those where the particle was initially vertical) as they contact with the bottom of the container. Some of the representations move up and down vertically after they contact with the bottom while others rotate and rebound on a tangent, even making contact with the wall of the container in some cases. These differences are caused by the uneven edge of the representations when they collide at an acute angle. The edges of each representation are not consistent between different cases, with the extent of differences determined by the size of component spheres and the method of clustering. Even for an individual representation, if different areas such as the crown of a sphere, or the space between the two spheres strike the bottom, the movement of the composite particle will vary from case-to-case. This could prove to be a significant problem in terms of obtaining reproducible packing structures from particles that are meant to be axially symmetric.

However, there does not appear to be clear correlation between accuracy of packing fraction and rebounding height and angle change. In other words, as far as packing fraction is concerned, differences in restitutional behavior of sphere-composites does not matter as much as initially feared.

3.5 Comparison of Clumped-Sphere Method (representation #7 & #8) with XMT Data

Figure 9

Figure 9 shows poured axial density profiles of the two cylindrical representations created using the smallest composite spheres (r=0.34mm; #7 and #8). The distance from the container base is scaled by the pellets' mean diameter. The CT data show only the middle, bulk section hence the profile drops at both ends. Results of clumped-sphere representations with low degrees of roundness (those built using 0.34mm radii spheres at the corner) agree the most closely with CT experimental data once end effects have dissipated (i.e., in the bulk of the bed). For packing structures created using these clumped spheres, mean bulk density was 0.582 (0.34mm, n=79) and 0.586 (0.34mm, n=120), which is respectively 1.5% and 0.9% lower than measured CT data, and 0.9% and 1.6% respectively higher than the voxel-based simulation results. The other cases of clumped sphere representations (those created using larger spheres) differ greatly from experimental values and also from representations #7 and #8, as observed in Figure 2.

Figure 10 displays radial density distribution for the same two cylindrical representations as previously reported for axial density distribution. Comparison between the two representations highlights that there is no significant difference between the predicted values of representation #7 and #8. The oscillation of the measured CT radial density profile is also presented. Close to the container wall, the radial density distribution varies in an oscillatory manner, with the amplitude of density oscillations becoming progressively damped with increasing distance from the container wall. This occurs due to the packing structure becoming more random as the ordering influence of the container wall dissipates. Assessing the measured profile against the predicted values, the sphere-composite model fails to predict the oscillatory behaviour, with the predicted profiles generally flat, bisecting the peaks and troughs of the measured result.
Figure 10

3.6 Comparison of Voxel-Based Simulations and XMT Data

Figures 11 & 12 compare the voxel-based simulated local packing results with CT measured data. The radial density distributions of the poured beds (Figure 11) show that the voxel-based simulation qualitatively predicts the mean profile of the CT scanned bed. The maximum radial density value for both packing model and the CT bed occurs at approximately 1-1.5 particle diameters, and the minimum radial density, excluding the value at the wall, occurs at approximately 2-2.5 particle diameters into the packing matrix. However, the voxel-based model under-predicts the CT measured profile, particularly in the near-wall region. Further into the bulk of the packing the difference between the two profiles reduces, although it always under-predicts the measured profile.

Fig 11
Fig 12

Axial density distribution profiles of voxel-based and CT-measured profiles are presented in

Figure 12. As with the sphere-composite comparison (Fig. 9), the DEM-predicted axial profile underestimates that of the CT-measured data. For the packed column considered in this work, several factors can contribute to the discrepancies between measured and predicted results and *also* between both prediction models. Both CT-scanned and voxel-based simulated structures contain digitization errors. For the sake of speed, simulations were performed at a lower resolution than for the CT scans (0.096 mm/voxel for CT scanned beds vs 0.197 mm/voxel for voxel-based method). Although performed at a lower resolution than the experimental CT measurements, the simulations were undertaken at a fine enough resolution to capture shape detail, ensuring that digital particle volume error was <1%. A volume conservation procedure is also employed to ensure that these errors do not accumulate, but it does not guarantee that pixel-level morphology is preserved at the same time. In the voxel-based method, pellets are input in digitized form and rotated digitally, although the voxels never change alignment (i.e., they do not rotate with the objects that they represent). The effects of a second type of error are more difficult to quantify in a random packing; in voxel-based simulations, because contact forces are calculated at the pixel-level, an extra pixel here and a missing pixel there on a particle surface can make a difference in the calculated net force/torque. Such errors are inherent in the digital approach, no matter how high the resolution is. Further investigation and algorithmatic improvement are needed as such errors are not present in CT-scanned structures.

3.7 Discussion

Averaged comparisons of scanned and simulated packed beds consisting of axially symmetric cylinders are reported. Multiple beds were scanned (4) and at least as many simulations were performed using both the voxel-based method and the sphere-composite method. Although discretized, the solutions represent a continuous and, in between collisions, smooth movement. During each time step, the direction and extent of particle movement and rotation are determined by particle interaction forces. Following initial setup, subsequent movements of each particle (which way to move and rotate at each time step and by how much) are governed by Newton's equations of motion that take into account gravity, friction and contact forces. Friction and contact forces arise at points of contact. These forces are calculated and prevent excessive overlaps between particles while they are under the influence of gravity. Thus, geometrical constraints determine how many and how balanced the contact forces are. Given the differences between algorithms and the random nature of the simulations, we do not expect an exact match in packing results, but what we see is a broad agreement between the two (where correct 'resolution' is selected), with the differences in axial packing density and bulk packing fractions largely attributable to the way geometric objects are represented in the respective simulation models.

The pouring of particles was simulated by introducing a small number of pellets each time from random points within a circular area above the container (which also had a circular cross section). This approach was in line with how pellets were introduced in the packing experiments, with pellets poured into the container a handful at a time, with no tapping, vibration, or shaking of the bed. Pellets were packed up to the top of the container and the bed was scanned using the Phoenix Nanotom.

TABLE 6

The bulk packing densities (excluding end effects) of the voxel-based, the CT-scanned bed and the eight cylinder representations formed using the sphere-composite method are compared in Table 6. The two simulation models selected have much in common: particle movements (deterministic trajectories in continuous space); process scenario (granular flow); sense of time and effects of impact and inertia. The mean bulk densities were obtained by averaging the axial density profiles in the middle section of the packed columns (i.e., in terms of vertical height). Standard deviations (stdev in Table 6) were also calculated from the axial density profiles. They are a measure of density variations within the packed beds, not between the beds. In other words, these stdev values are an indicator of how uniform the bed structures are in the middle (i.e., bulk) section in each case. Based on the XMT data, the mean bulk density was estimated to be 0.591. In terms of voxel-based simulations, which were carried out at one-half the scale of the scan resolution, bulk density was calculated as 0.577, 2.37% lower than the mean determined for the experimental beds. For the clumped-sphere method results, whereby 8 different particle representations were investigated, there is a difference of 20% between the highest and the lowest predicted bulk density values. When all eight representations are compared with CT data, the range of difference is between -1.5% and 18.1%. However, the two cylinder representations formed using r=0.34mm (the smallest composite spheres used to build cylindrical particles) demonstrate a significant improvement over the other 6 representations. The values for #7 and #8 still under-predict bulk packing fraction, but the values are closer to CT measured data than those of the voxel-based method. The level of density fluctuation within the CT-scanned beds is approximately one-half of that of the voxel-based simulated values (0.006 versus 0.014 respectively). The increased fluctuation in the voxel-based simulated beds is attributed to the fact that these simulations were performed at one-half the scale for the sake of speed. Lower resolution usually results in higher digitization errors, which can be further amplified during simulation by particle rotation. The amount of fluctuation within the packed beds created using the clumped sphere method is marginally higher than that of the mean voxel-based results, with values ranging between 0.019 and 0.026.

In addition to bulk and local (axial and radial) packing fractions, it was decided that the axial orientation distribution of the pellets would be an appropriate metric for our purposes rather than other structural metrics, such as two-point correlation functions (Torquato, 2001). This is particularly the case for the clumped sphere method pellet representations, some of which contain internal pore spaces, as two-point correlation function statistics lump together contributions from both intra- and inter-pellet pore structures. Figure 14 compares vertical pellet orientation distributions for poured packed beds as calculated from clumped sphere method, voxel-based method and CT structures using the modified Markov chain Monte Carlo (MCMC) procedure (Gilks et al. 1996). Here, angle refers to the acute angle between a particle's polar axis and the packed column's vertical axis.

Fig 13

The plots shown in figure 13 provide particle orientation distribution for the bed as a whole. The CT beds exhibit a high proportion of pellets oriented toward the midrange angle groups, in the form of an inverted V shape. In the clumped-sphere method experiments, the orientation distribution of only a single cylinder representation is reported. The reason for this is that mean variation in frequency vs angle range was just 1.66% (stdev = 0.608) across all 8 clumped-sphere representations, with no obvious trend for different pellet representations. The orientation distribution of the sphere-composite representation exhibits a largely uniform trend, with frequency values increasing monotonically with angle. Compared to the XMT data, there are an excessive proportion of pellets in the 80-90° group. For the voxel-based method, a slight improvement is seen in the quantitative prediction of particle orientation over that of clumped-sphere method results, when compared against XMT data, although notable discrepancies still exist in the minimum and maximum angle groups.

There are two plausible reasons for the differences between predictions and measured data in terms of the frequency of particles residing in the high angle groups. One is wall effects. The presence of horizontal (bottom) and vertical (side) walls may encourage axially symmetrical particles to adopt either vertical or horizontal orientations as these two orientations are more stable against the wall (Zhang et al. 2006). However, the presence of a solid wall did not cause a high frequency of pellets in the 80-90^{o} range for XMT results, suggesting wall effects may not be the sole cause. The other reason possibly has to do with particle representation; specifically, for the voxel-based method - digitization errors, as discussed in Section 3.6. For the clumped-sphere method, the pellets were created from sphere-composites and all have non-smooth, undulating surfaces compared to the real pellets, with different representations having varying levels of fidelity. With the presence of a retaining structure such as a wall, pellet orientation is more stable when in a near-vertical orientation. When combined with close contacts between other pellets, this makes rearrangement once ordered against the wall less likely, leading to an increase in the highest angle group.

4. Conclusions

Beds of cylindrical alumina pellets were packed, tomographically scanned and the results compared with simulation values obtained using two commercial versions of DEM code: one that uses sphere- composites to represent particle shape, the other voxel-based. The comparison was performed in terms of bulk packing density, axial and radial density profiles and pellet orientations.

The clumped-sphere model is dependent on creating complex multi-element model particles from adequate numbers of spherical elements, while the voxel-based version builds particles at the voxel level. In practice, a voxel is at least an order of magnitude smaller than the primary spheres. A range of sphere-composite representations of a cylinder are compared, which the interested reader can use to obtain guidelines. Of the eight sphere-composite representations reported, representation #7 and #8, those which use the smallest sphere radii (0.34mm)

qualitatively follow the experimentally-measured trend most closely.

A range of factors that in theory could affect accuracy of the simulation results have been examined in detail, including edge roundedness, surface roughness and restitutional behaviour as a function of sphere-composite representations. Edge roundedness appears to have a more significant effect on the packing structure than others. Results of representations with low degrees of roundness agree most closely with the laboratory experiments in terms of axial and radial packing densities. In terms of orientation distribution, there was no significant difference between the two approaches to shape representation, although voxel-based representation gives closer match with experimental data. If particle shape requirements were to become more geometrically complicated than the small, flat-ended cylinders, then using the clumped sphere method would be expected to require smaller, higher numbers of primary spheres to attain the accuracy of particle shape. In the voxel-based method, simulation time is largely determined by the number of voxels used to build the particles, as opposed to the number of particles. As such highly-complex particles pose little, if any additional simulation cost. In this sense, the voxel-based method is more computationally efficient for packing of complex shapes.

Since particle shape influence packing structure, it follows that how precise the shape is represented, especially at the corners and edges, can significantly affect the accuracy of the simulation results. Due to the obvious computational penalty, it is a common practice, and indeed the desire of sphere-composite users, to use as few element spheres as possible to represent a given shape, without bothering to investigate or realising the impact of their choices. The case studies reported here serve to illustrate just how much influence there can be. The conclusion therefore is that, for packing at least, matching the object's overall shape and dimensions is not enough, only when a high enough resolution is used for corners and edges, could the sphere-composite approach possibly match the experimental data quantitatively.

5. References

Aste T, Weaire D. The pursuit of perfect packing, 2nd edn. CRC Press, Taylor & Francis Group. 2008. ISBN: 13: 978-1-4200-6817-7.

Barrett PJ. The shape of rock particles, a critical review. Sedimentology 1980; 27(3): 291-303.

Caulkin R, Ahmad A, Fairweather M, Jia X, Williams RA. Digital predictions of complex cylinder packed columns. Comp & Chem Eng 2009a;33(1):10-21.

Caulkin R, Jia X, Xu C, Fairweather M, Williams RA, Stitt H, Nijemeisland M, Aferka S, Crine M, Léonard A, Toye D, Marchot P. Simulations of structures in packed columns and validation by X-ray tomography. Ind Eng Chem Res 2009;48:202-213.

Caulkin R, Islam MS, Jia X, Fairweather M. Studies for the development of a virtual permeameter. Comp & Chem Eng 2014;68:190-202.

Cundall P A, Strack ODL. A discrete numerical model for granular assemblies. Geotechnique 1979;29(1):47-65.

Dyskin AV, Estrin Y, Kanel-Belov AJ, Pasternak E. Toughening by fragmentation - How topology helps.

Adv Eng Mat 2001;**3**(11):885-888.

Favier JF, Abbaspour-Fard MH, Kremmer M, Raji AO. Shape representation of axi-symmetrical, non-spherical particles in discrete element simulation using multi-element model particles. Eng Comp 1999;16(4):467-480.

Gilks WR, Richardson S, Spiegelhalter DJ. Marko chain Monte Carlo in practice; Chapman & Hall: Boca Raton, FL; 1996.

Günther J, Schmitz P, Albasi C, Lafforgue C. A numerical approach to study the impact of packing density on fluid flow distribution in hollow fiber module. J Membrane Sci 348;2010:1(2): 277-286.

Goodling JS, Vachon R I, Stelpflug WS, Ying SJ, Khader MS. Radial porosity distribution in cylindrical beds packed with spheres. Powder Tech 1983;35(1): 23-29.

Hertz H. On the contact of elastic solids. J fur die Reine und Angewandte Mathematik 1982;92: 156-171.

Höhner D, Wirtz S, Kruggel-Emden H, SchererV. Comparison of the multi-sphere and polyhedral approach to simulate non-spherical particles within the discrete element method: Influence on temporal force evolution for multiple contacts. Powder Tech 2011; 208(3):643-656.

Jia X, Williams RA. A packing algorithm for particles of arbitrary shapes. Powder Tech 2001;120(3): 175-186.

Jia X, Caulkin R, Williams RA, Zhou ZY, Yu AB. The role of geometric constraints in random packing of non-spherical particles. EPL 2010;92:68005.

Jung S, Ehlert S, Mora J-A, Kraiczek K, Dittmann M, Rozing GP, Tallarek U. Packing density, permeability, and separation efficiency of packed microchips at different particle-aspect ratios. J Chromatography A 2009;1216(2): 264-273.

Kodam M, Bharadwaj R, Curtis J, Hancock B, Wassgren C. Force model considerations for glued-sphere discrete element method simulations, Chem. Eng. Sci. 64 (2009) 3466-3475.

Kodam M, Bharadwaj R, Curtis J, Hancock B, Wassgren C.Cylindrical object contact detection for use in discrete element method simulations, Part II-Experimental validation. Chem Eng Sci 2010;65(22): 5863-5871.

Kubie J. Influence of containing walls on the distribution of voidage in packed beds of uniform spheres.Chem Eng Sci 1988;43:1403-1405.

McGreavy C, Foumeny EA, Javed KH. Characterisation of transport properties for fixed beds in terms of local bed structure and flow distribution. Chem Eng Sci 1986;41: 787-797.

McNeely W, Puterbaugh K, Troy J. Six degree-of-freedom haptic rendering using voxel sampling. Computer Graphics Proceedings, ACM, August 1999; 401-408.

Mindlin RD, Deresiewicz H. Elastic spheres in contact under varying oblique forces. J Appl Mech 1953;20: 327-344.

Powell MJ. Computer-simulated random packing of spheres. Powder Tech 1980;25:45-52.

Richard P, Philippe P, Barbe F, Bourlés S, Thibault X, Bideau D. Analysis by X-ray microtomography of a granular packing undergoing compaction. Phys Rev E 2003;68:020301.

Santamarina JC. Soil behaviour: The role of particle shape. Proc Skempton Conf. London 2004.

Sasov AY. X-ray microtomography. Sov. J. Nondestr. Test. (Engl. Transl.); (United States); Journal Volume: 24:5; Other Information: Translated from Defektoskopiya; 24: No. 5, 23-30 (May 1988):315-321.

Seidler GT, Martinez G, Seeley LH, Kim KH, Behne EA, Zaranek S, Chapman BD, Heald SM. Granule-by-granule reconstruction of a sandpile from X-ray microtomography data. Phys Rev E 2000;62: 8175-8182.

Sharma S, Mantle MD, Gladden LF, Winterbottom JM. Determination of bed voidage using water substitution and 3D magnetic resonance imaging, bed density and pressure drop in packed bed reactors. Chem Eng Sci 2001;56:587-595.

Shimobe S, Moroto N. A new classification chart for sand liquefaction. Earthquake geotechnical Eng 1995;315-320.

Torquato S. Random heterogeneous materials: Microstructure and macroscopic properties. Interdisciplinary Applied Mathematics Series;Springer-Verlag: New York, 2001; Vol. 16.

Xu C, Jia X, Williams RA, Stitt EH, Nijemeisland M, El-Bachir S, Sederman A J, Gladden LF. Property predictions for packed columns using random and distinct element digital packing algorithms. Fifth World Congress on Particle Techy, Orlando, FL, Apr 23-27 2006.

Yang RY, Zou RP, Yu A.B. Computer simulation of the packing of fine particles. Phys Rev E 2000;62: 3900-3908.

Yang RY, Zou RP, Yu A.B. Numerical study of the packing of wet coarse uniform spheres. AIChE 2003;49:1656-1666.

Zhang W, Thompson KE, Reed AH, Beenken L. Relationship between packing structure and porosity in fixed beds of equilateral cylindrical particles. Chem Eng Sci 2006;61: 8060-8074.

Zou RP, Yu AB. Evaluation of the packing characteristics of mono-sized non-spherical particles. Powder Tech 1996;88(1): 71-79.

Table 1

	Sphere-composite	Voxel based	Surface mesh
Basic idea	A sphere is represented analytically by its centre and radius as (x,y,z,a); everything else by clamping spheres together	A shape is treated as 3D image, rather than geometry, as a coherent collection of voxels	The surface of a shape is wrapped by a triangular mesh
Motivations	Sphere is the easiest to deal with when detecting collisions and overlaps. Also memory efficient	Easy collision/overlap detection. Same format used for output from image based particle or structure characterisation equipment, thus no conversion required.	Method of choice for computer graphics (photorealistic shading), and finite element type analysis
Precision	Low, especially for sharp corners and flat surfaces. Easy to incorporate surface roughness if required, but costly	High, but staircases always exist for diagonal surfaces or edges	High, retains sharp corners and flat surfaces well. Difficult to incorporate surface roughness
Collision/overlap detection	Easy but time consuming	Easy and fast	Difficult and time consuming
Rotation	Direct transformation and fast. Building blocks (spheres) change orientation with the object	Direct transformation often creates small holes in solid surfaces. Indirect rotation is slow. Building blocks (voxels) do not change their orientations - they merely shift their locations	Direct transformation and fast. Building blocks (triangles) change orientation with the object
Contact force models	Several and specific to spheres	Currently only one (for the model used here): contact force is proportional to overlap volume.	Few
Ease of shape construction	Manually, through trial and error, to balance precision and computational cost	Automatic or directly from 3D imaging devices	Can be automatic

Table 2

Representation >	1	2	3	4	5	6	7	8
Radius of each element sphere (mm)	0.84	0.80	0.74	0.47	0.47	0.57	0.34	0.34
Total number of element spheres	27	27	27	125	85	35	120	79
Total number of particles in packed column	3943	3929	3913	3586	3726	4023	3342	3351

Table 3

Roundness	Mean Volume Packing Fraction	Sphere radius (mm), No. of element spheres
0.20	0.582	0.34mm, n=79
0.20	0.586	0.34mm, n=120
0.28	0.623	0.47mm, n=85
0.28	0.652	0.47mm, n=125
0.33	0.698	0.57mm, n=85
0.43	0.685	0.74mm, n=27
0.47	0.682	0.80mm, n=27
0.49	0.686	0.84mm, n=27

Table 4

Surface roughness	Volume packing fraction	Sphere radius (mm), No. of element spheres
0.11	0.652	0.47mm, n=125
0.17	0.586	0.34mm, n=120
0.27	0.686	0.84mm, n=27
0.28	0.582	0.34mm, n=79
0.29	0.698	0.57mm, n=35
0.30	0.682	0.80mm, n=27
0.35	0.685	0.74mm, n=27
0.57	0.623	0.47mm, n=85

Table 5

Initial particle angle (when dropped) →	2^o (upright)		45^o	
Sphere-composite representation↓	Angle (deg) at contact point with base (0.11s) / and rebound angle (0.1s later)	Rebound height	Angle (deg) at contact point with base (0.11s) / and rebound angle (0.1s later)	Rebound height
0.8mm, n=27	5.78 / 104.74	0.00184	45.22 / 45.49	0.00068

0.84mm, n=27	5.23 / 97.04	0.00166	45.50 / 56.11	0.00281
0.74mm, n=27	4.63 / 84.94	0.00465	40.90 / 72.29	0.00390
0.57mm, n=35	5.82 / 102.65	0.00324	46.56 / 72.81	0.00719
0.47mm, n=125	7.60 / 129.52	0.00256	45.65 / 49.40	0.00269
0.47mm, n=85	7.23 / 139.80	0.00203	46.04 / 57.21	0.00310
0.34mm, n=120	8.20 / 130.36	0.00284	45.72 / 50.80	0.00236
0.34mm, n=79	8.15 / 129.54	0.00283	45.80 / 51.64	0.00247

Table 6

Case	Mean bulk density (stdev)	% difference from CT
#1 (0.84mm, n=27)	0.686 (0.021)	16.07%
#2 (0.8 mm, n=27)	0.682 (0.020)	15.40%
#3 (0.74mm, n=27)	0.685 (0.020)	15.91%
#4 (0.47mm, n=125)	0.652 (0.021)	10.32%
#5 (0.47mm, n=85)	0.623 (0.016)	5.41%
#6 (0.57mm, n=35)	0.698 (0.022)	18.10%
#7 (0.34mm, n=120)	0.586 (0.026)	-0.85%
#8 (0.34mm, n=79)	0.582 (0.019)	-1.52%
Voxel-based method	0.577 (0.014)	-2.37%
Experiment (CT)	0.591 (0.006)	-

Figure 1. Illustration of eight different representations of the cylindrical particles (a) top view, (b) ¾ side view.

Figure 2. Radial volume packing fraction of the bed with eight representations.

Figure 3. Axial volume packing fraction of the bed with eight representations.

Figure 4. Quantification of particle roundness (D_s/D_i).

Figure 5. Effect of particle roundness on packing structure.

Figure 6. Radial volume packing fraction of original particles and modified particles.

Figure 7. Quantification of surface roughness.

Figure 8. Relationship of surface roughness and volume packing fraction.

Figure 9. Axial packing fraction results from clumped sphere method and XMT.

Figure 10. Radial packing fraction results from clumped sphere method and XMT.

Figure 11. Radial packing fraction results from voxel-based method and XMT.

Figure 12. Axial packing fraction results from voxel-based method and XMT.

Figure 13. Vertical orientation distributions by clumped sphere method (representation #7), voxel-based method and XMT.

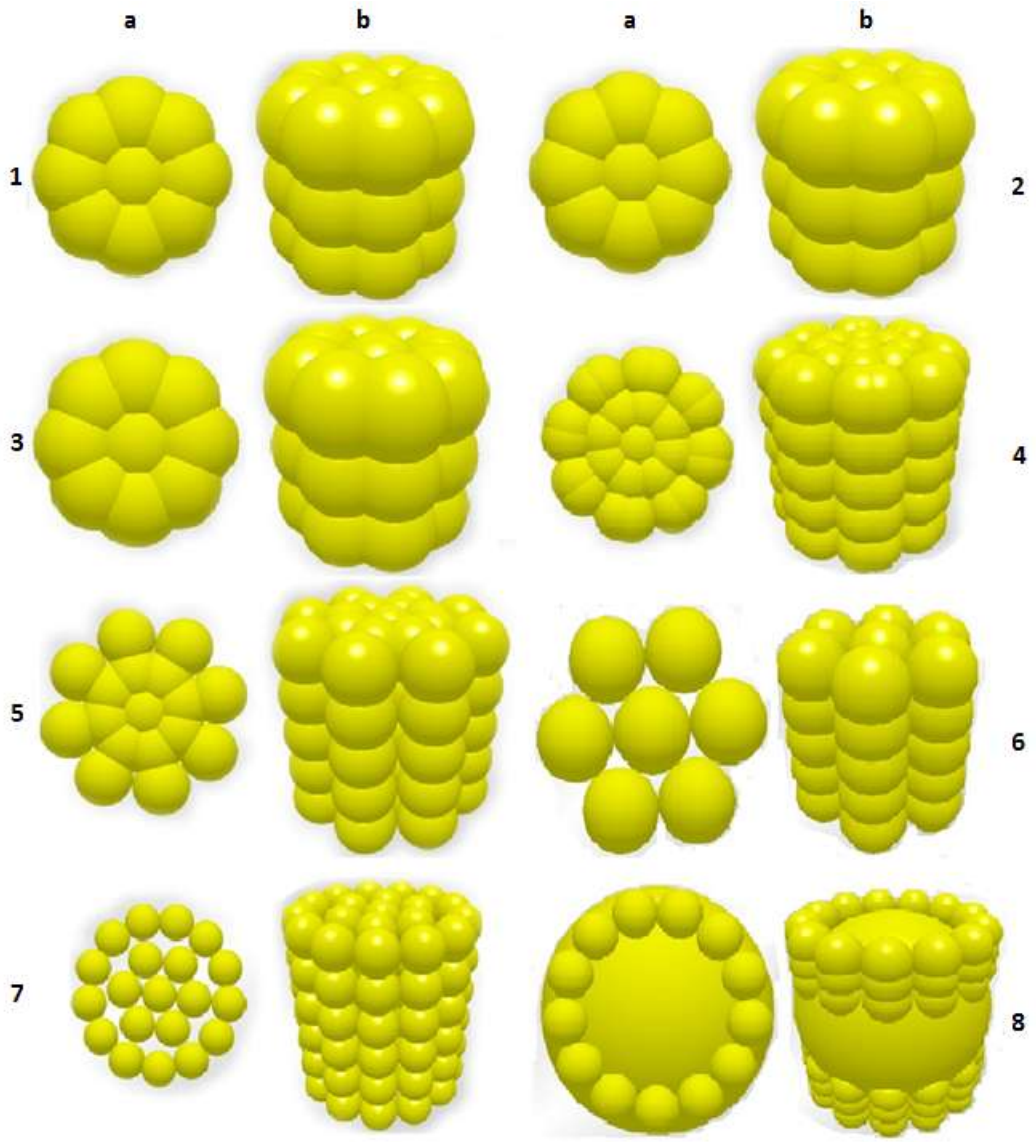

Figure 1

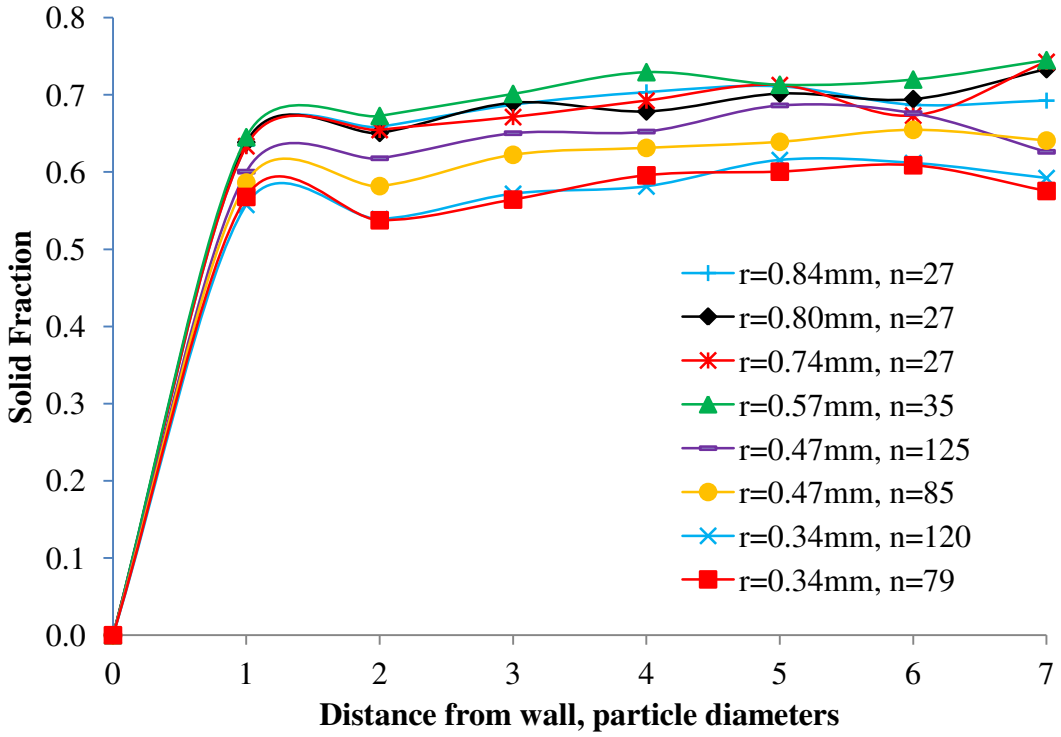

Figure 2

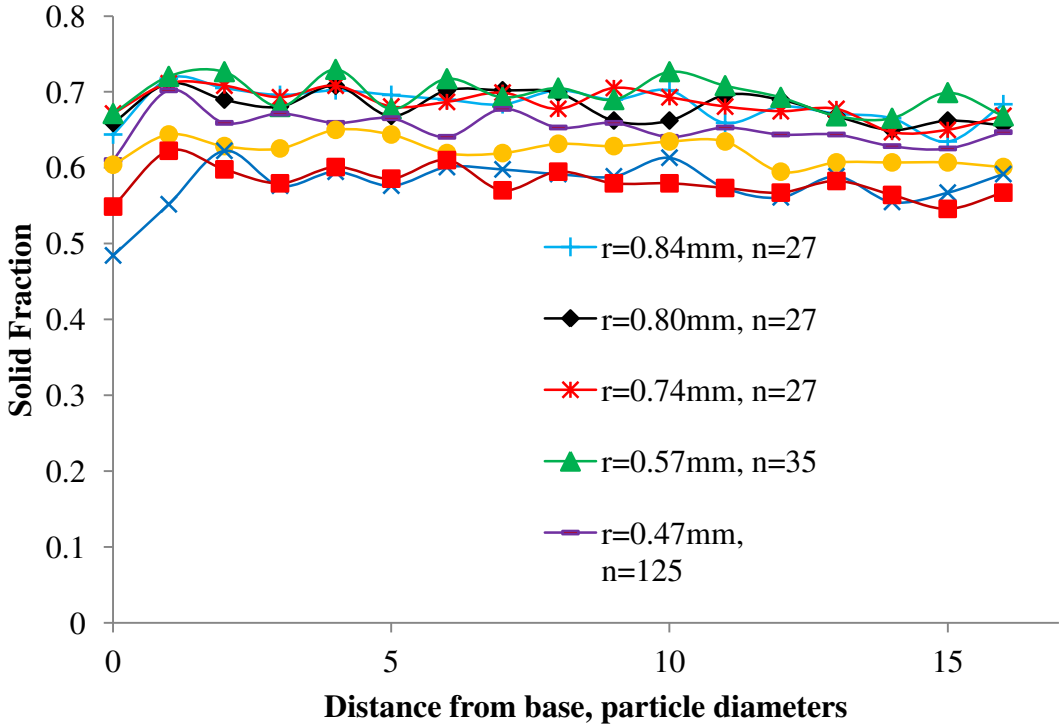

Figure 3

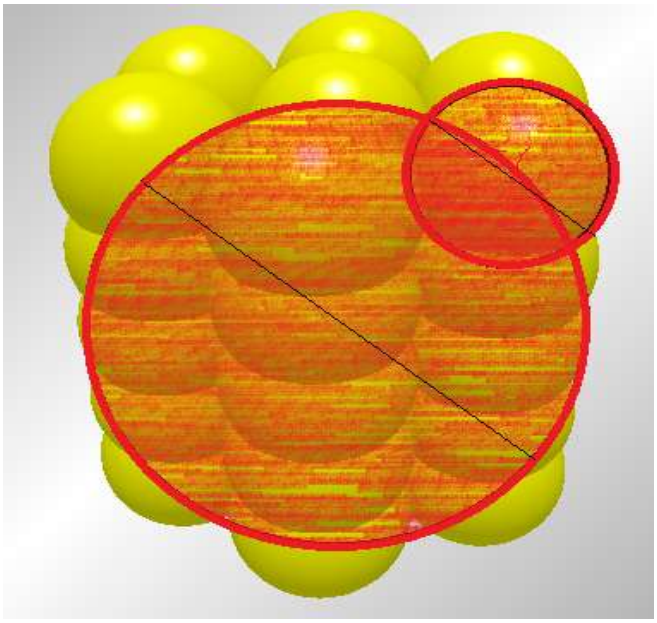

Figure 4

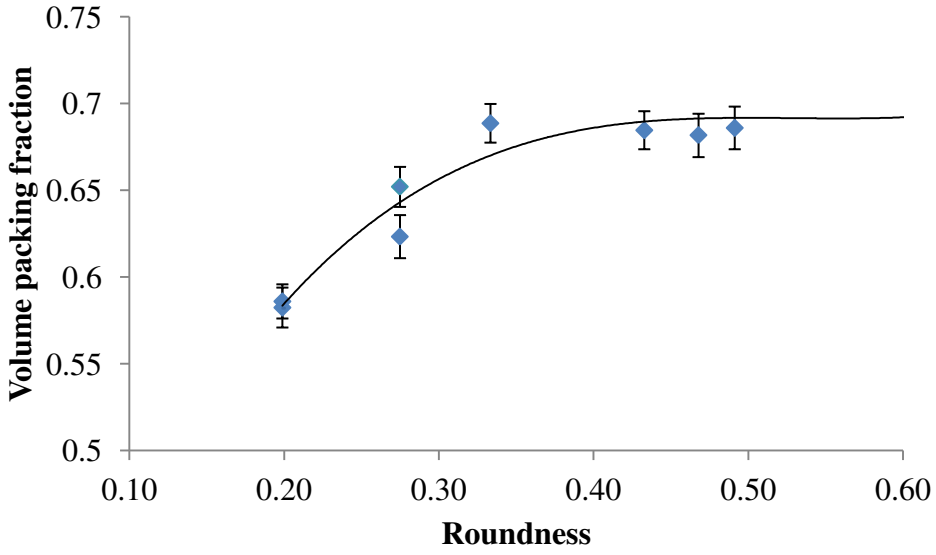

Figure 5

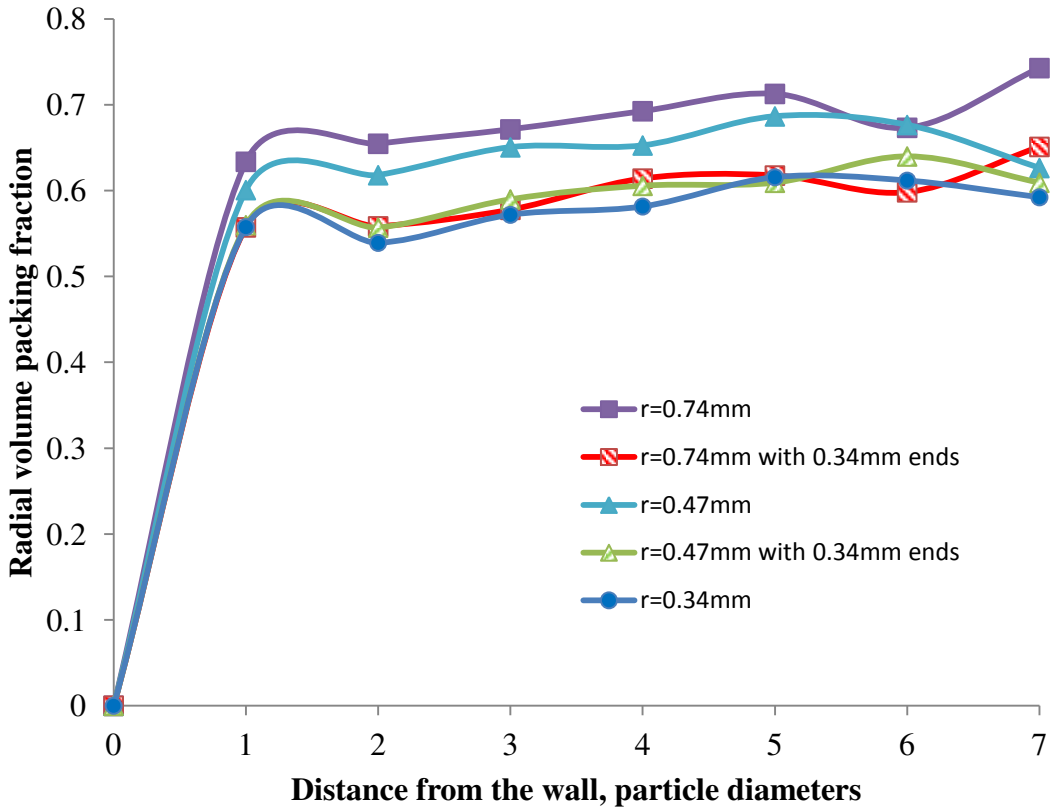

Figure 6

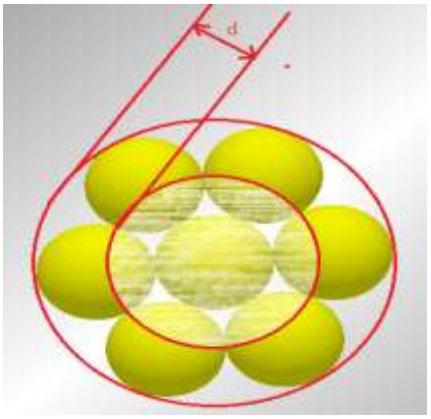

Figure 7

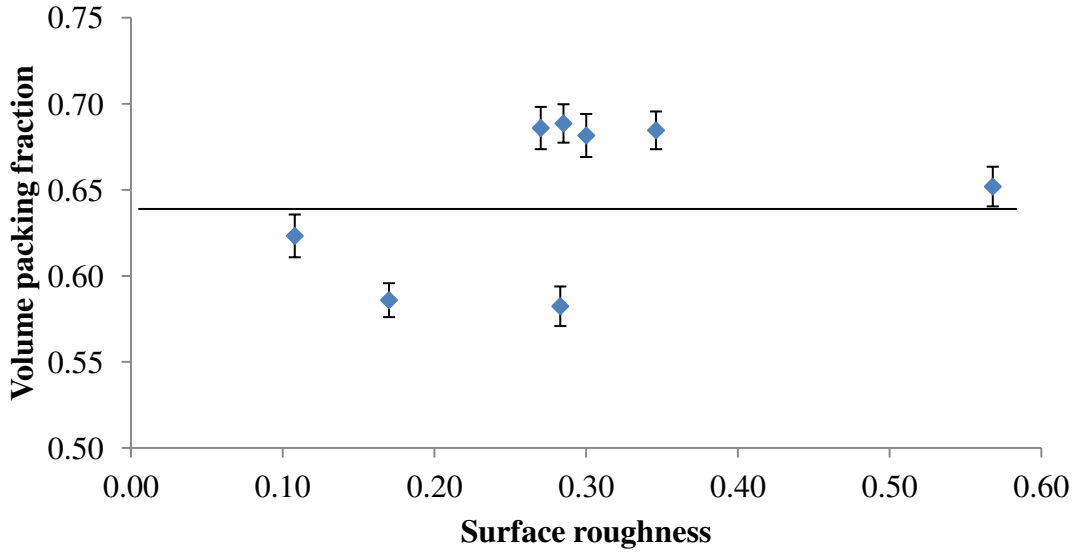

Figure 8

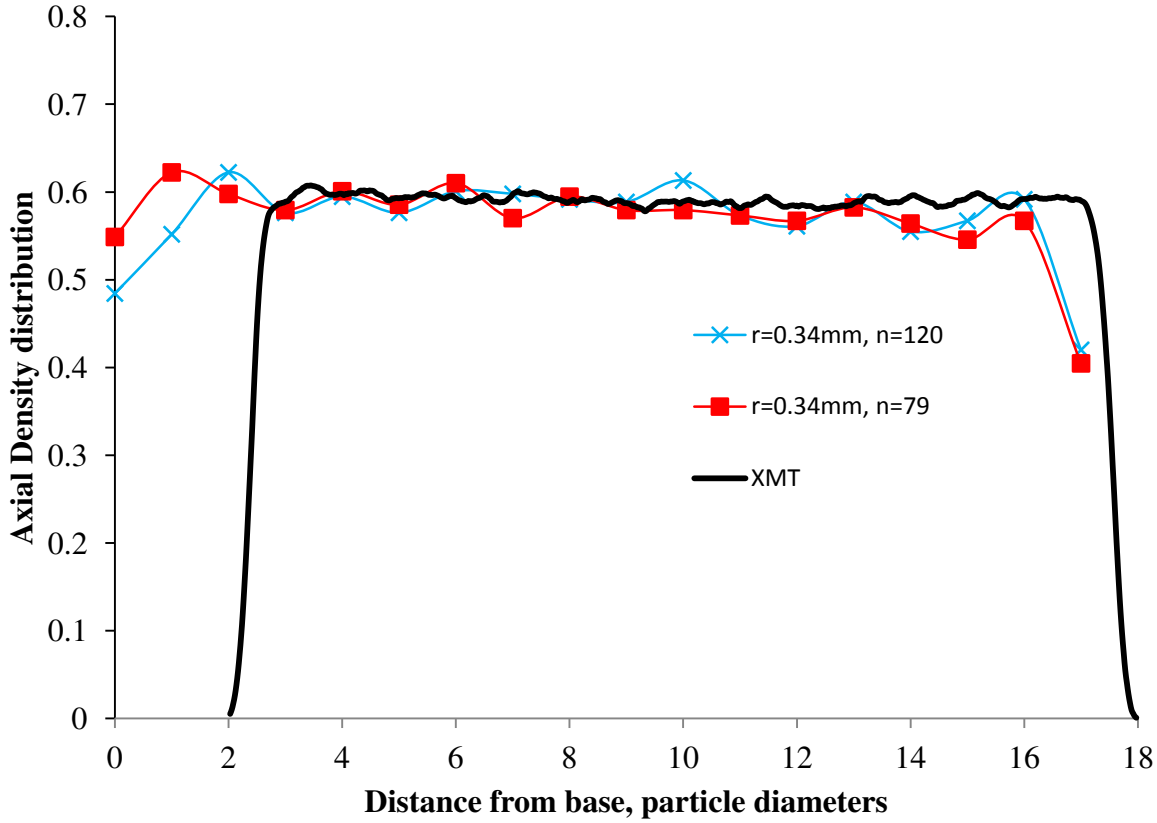

Figure 9

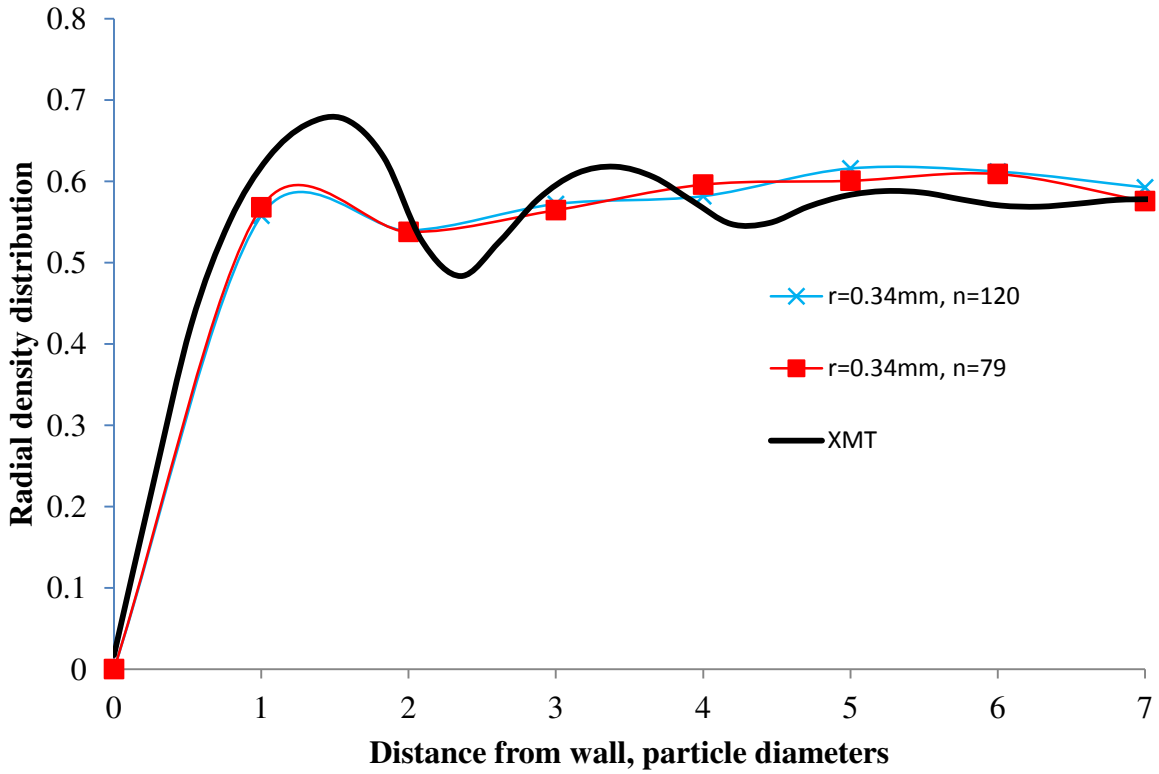

Figure 10

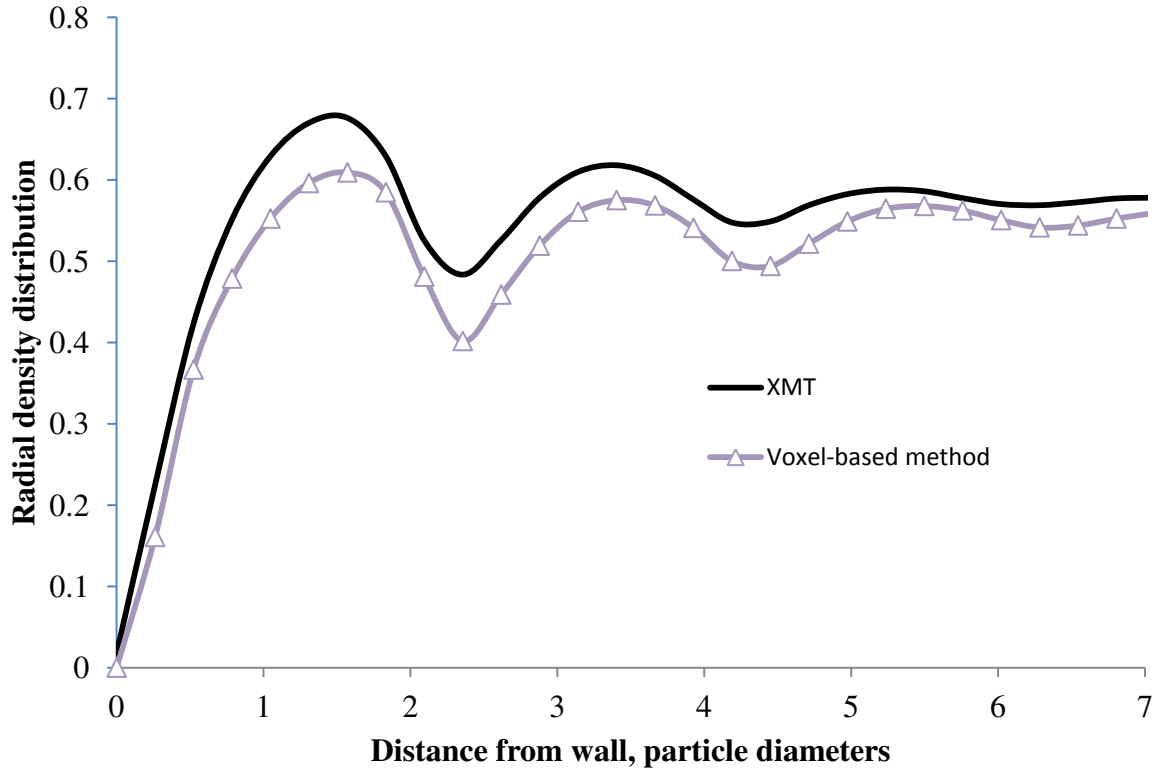

Figure 11

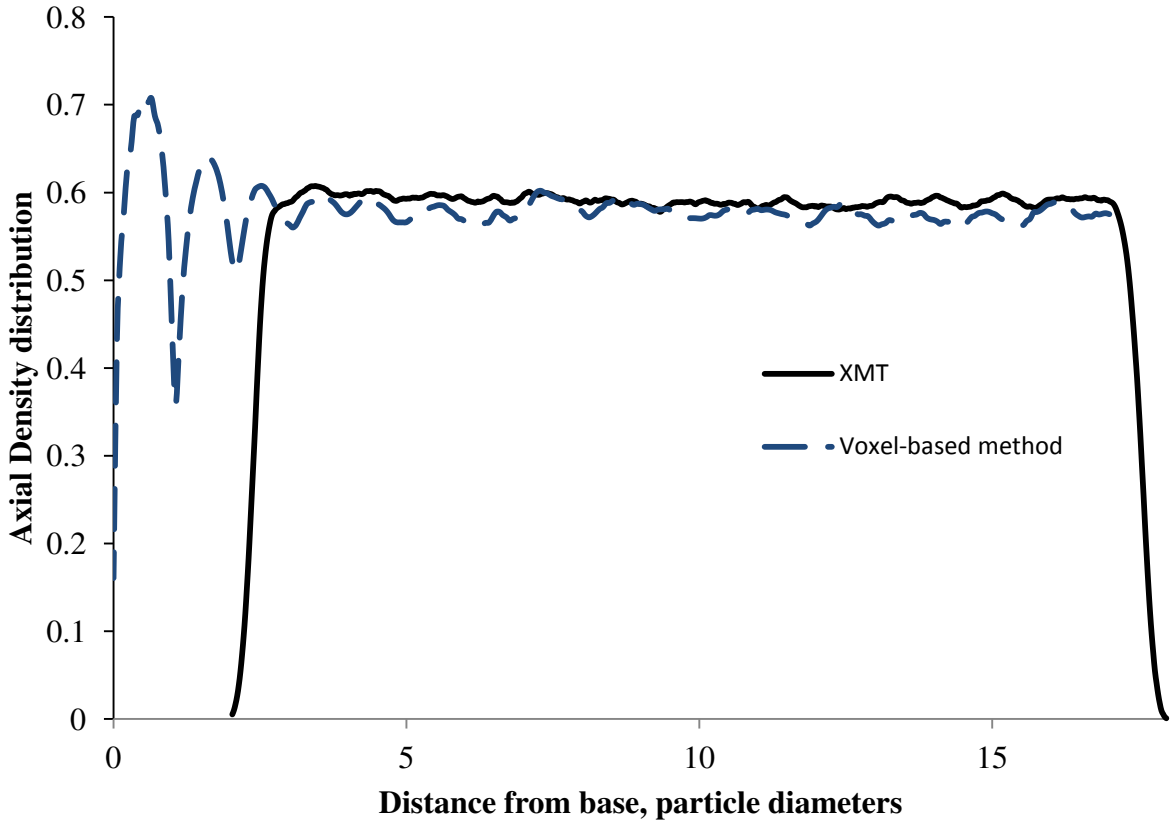

Figure 12

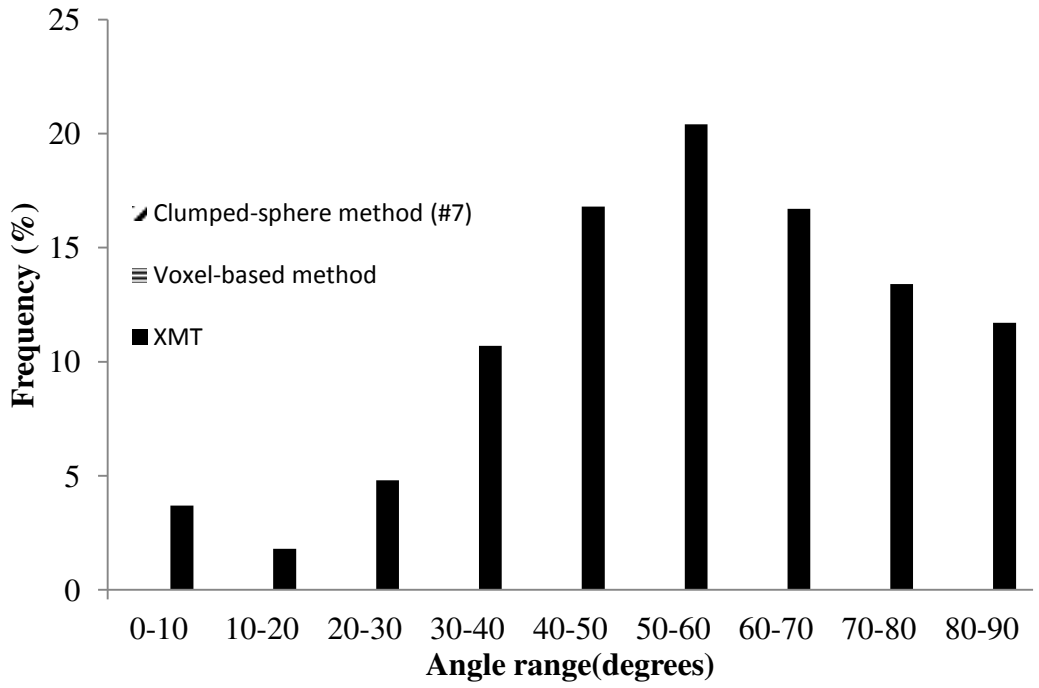

Figure 13

Figure Captions: